IEEE Access
Multidisciplinary | Rapid Review | Open Access Journal

Received March 11, 2019, accepted March 25, 2019, date of publication March 29, 2019, date of current version April 16, 2019.

Digital Object Identifier 10.1109/ACCESS.2019.2908212

An Adaptively Controlled 10-Output Reconfigurable Dual-Bus SIMO System With Group Allocator for Diversified Load Condition

SE-UN SHIN, (Member, IEEE)
Department of Electrical Engineering and Computer Science (EECS), University of Michigan, Ann Arbor, MI 48109, USA
e-mail: seuns@umich.edu

ABSTRACT Portable electronic devices require multiple supply voltages with relatively large differences in load currents, causing serious regulation, EMI, and efficiency problems when adopting a single-inductor multiple-output (SIMO) dc-dc converter. To resolve these issues, this paper presents a reconfigurable SIMO system with ten-output having two buses, one for heavy-load and one for light-load outputs. The converter maintains the load current condition so that each bus is well balanced even when the load currents are diversified by using the proposed group allocator, which properly assigns a bus for each output depending on its load current. Due to this load balancing function, regulation issues that could occur under diversified load conditions are resolved, and high efficiency is achieved over a wide load current range. The test chip was fabricated in 1P4M 0.18 μm CMOS process. The system has ten independently regulated outputs with an output voltage ripples below 25 mV, and greater than 81% efficiency is achieved across a wide load range (0–300 mA).

INDEX TERMS SIMO converter, group allocator, diversified load condition, load balancing function, voltage ripple, dc-dc converter, all comparator-based control, adaptive pulse modulation.

I. INTRODUCTION

Multiple supply voltages with different voltage levels are required for various function blocks in modern VLSI systems. For example, in a mobile system, digital circuit blocks require low-level supply voltages to reduce dynamic power loss, while analog circuit blocks, such as audio/RF amplifiers, require mid-level supply voltages for acceptable performance and reliability. For I/O circuits and display modules, relatively high-level supply voltages are necessary [1]–[5].

As the number of different supply voltages increases, the number of single-inductor single-output (SISO) DC-DC converters should also be increased as shown in Fig. 1(a). This is a burden on the system since the same number of inductors are required as converters. Thus, the volume and cost are increased due to additional pads and pins as well as the additional inductors themselves. To reduce the volume and cost, a single-inductor multiple-output (SIMO) converter was developed as shown in Fig. 1(b). It allows only a single inductor to regulate multiple outputs with different voltage and current levels. Therefore, the SIMO converter reduces not only the required number of inductors but also the number of pins and pads. However, there are more issues associated with SIMO converters than with SISO converters, such as poor cross regulation, slow load transient, large ripple, low current capability, instability, and efficiency degradation [6]. Moreover, a control method for the power delivery sequence of multiple outputs is required. Therefore, much research has focused on developing SIMO control methods [7]–[16].

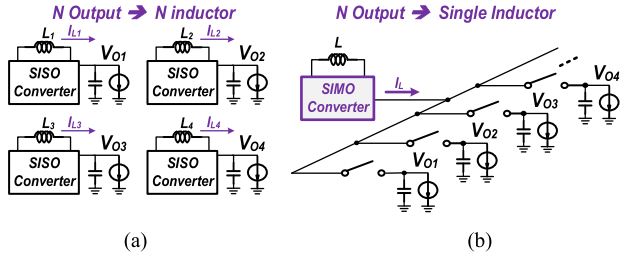

FIGURE 1. (a) SISO converter and (b) SIMO converter for multiple outputs.

First, time-multiplexing control (TMC) was presented as a control method for multiple outputs for SIMO converters in [7]–[9]. In TMC, the N outputs are independently controlled and regulated with N feedback loops for each

The associate editor coordinating the review of this manuscript and approving it for publication was Shravana Musunuri.

output. However, complex N compensators are required for N outputs. Also, energy is supplied to one pre-ordered output per single switching cycle (T_{SW}). This method causes a low transient response, large output voltage ripple, and low power delivery capability. To resolve the low performance of TMC, an ordered power-distributive controlled (OPDC) SIMO converter was presented in [10]–[12]. It supplies the inductor current (I_L) to all outputs during a single T_{SW}. Thus, the OPDC SIMO converter has fast load transient response and relatively small ripple. The control for all outputs is simply conducted using PI control of the last output, which integrates the total error of all outputs, while the other outputs are self-controlled by the comparator. However, there is a stability issue and low cross regulation depending on the last output load condition since the main control loop uses only the error of the last output. To resolve the poor cross regulation, a control with an energy recovery duration in every T_{SW} was presented in [13]. Since this energy recovery duration buffers the cross regulation in the load transient state, all output voltages can be independently regulated with minimized cross regulation. However, because an additional switch is needed for the energy recovery duration, there is unnecessary conduction loss in every T_{SW}, reducing the total power efficiency.

To achieve high efficiency and low cross regulation at the same time, an all comparator-based control (ACBC) in which all outputs are controlled by comparators, including the last output, was presented in [14]–[15]. Since all outputs are controlled by the comparator, it shows good cross regulation performance and fast transient response by instantaneous variation of the switching frequency only in transient state. In contrast, in the steady state, a phase-locked loop allows the converter to operate with a fixed frequency again. Since the ACBC does not require an additional switch, high efficiency can be achieved. Therefore, ACBCs are one of the most popular solutions for SIMO converters to date. On the other hand, an adaptive pulse modulation (APM) control using gm-cells instead of comparators connected at each output was presented recently for use in SIMO converters when there are many light-load outputs [16]. The power efficiency increases under light-load conditions owing to the variation in the switching frequency, which is dependent on the load current.

Although both ACBCs and APMs perform well as SIMO controllers, there are still practical issues due to the strong dependency on the load condition, which randomly varies with the operation of the loading block. These issues limit the practical application of SIMO converters. More details on these load condition issues will be given in the following section.

In this paper, which is an extension of [21], a new SIMO system is presented that utilizes a converter referred to as a dual-bus multiple-output (DBMO) converter, which allocates appropriate control to each output depending on the load current, thus resolving the practical issues associated with SIMO converters.

The rest of the paper is organized as follows. The load condition concerns associated with SIMO converters are introduced in Section II. Section III presents the proposed DBMO converter. Section IV presents the circuit implementation for the proposed converter, and Section V provides the measurement results. Finally, the paper concludes in Section VI.

II. PRACTICAL LOAD CONDITION ISSUES OF SIMO CONVERTERS

A. ALL COMPARATOR-BASED CONTROL

An ACBC is preferred over other types of controllers for use in SIMO converters because of its simple control and low cross regulation. Fig. 2 shows a SIMO converter with ACBC; the regulations of all the outputs are self-controlled. In other words, when an output voltage is charged to a reference voltage, the corresponding output switch is turned off, and the next output switch is sequentially turned on to transfer the inductor energy to the next output. However, despite the advantages of ACBC, many issues occur when light-load currents exist among the outputs.

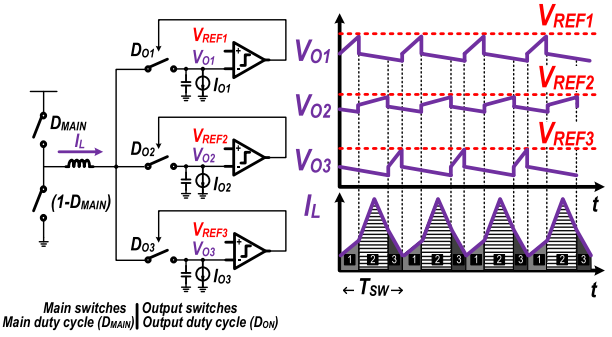

FIGURE 2. SIMO converter with all comparator-based control.

1) MINIMUM ON-TIME PROBLEM

The output duty cycle (D_{ON}) of the output switch is used to regulate the output voltage in a SIMO converter. However, when light-load output exists in ACBC, significant regulation problems can occur due to the delay from the comparator to the gate of the output switch. Moreover, a minimum on-time ($T_{ON,MIN}$) in the output switch control is required for switching noise insensitivity. Thus, some delay (d_{in}) is inserted to ensure the stable operation of the comparator until the switch is turned off. Considering $T_{ON,MIN}$ and the desired on-time ($T_{ON,DESIRED}$), the desired output duty ($D_{ON,DESIRED}$) for each output switch is expressed as follows:

$$T_{ON,MIN} = d_{par} + d_{comp} + d_{gd} + d_{in} \quad (1)$$

$$D_{ON,MIN} = T_{ON,MIN}/T_{SW} \simeq I_{O,MIN}/I_L \quad (2)$$

$$D_{ON,DESIRED} = T_{ON,DESIRED}/T_{SW} \simeq I_{O,DESIRED}/I_L \quad (3)$$

where d_{par}, d_{comp}, d_{gd}, d_{in}, $D_{O,MIN}$, $I_{O,MIN}$, and $I_{O,DESIRED}$ represent the parasitic delay, comparator delay, gate driver delay, inserted delay, minimum output duty, minimum load

current, and desired current for the load, respectively. If $D_{ON,DESIRED} < D_{ON,MIN}$, i.e., $I_{O,DESIRED}$ for the regulation of the light-load output is lower than the supportable $I_{O,MIN}$ in the SIMO converter, regulation failure occurs because of overcharging at light-load output as shown in Fig. 3 (a).

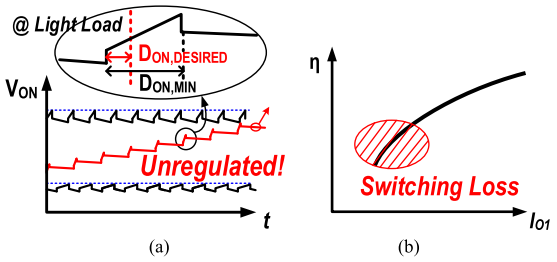

FIGURE 3. (a) Minimum on-time problem, (b) low efficiency issue in SIMO converter with all comparator-based control.

2) EFFICIENCY

Since the ACBC supplies energy to the outputs sequentially according to a pre-defined order, the light-load outputs that do not require frequent energy delivery also experience frequent switching. This results in unnecessary switching loss and therefore power efficiency degradation as shown in Fig. 3 (b). To improve the light-load efficiency, adaptive control of the output switching frequency is necessary [17].

3) SWITCHING NOISE

Switching noise appears when the output switches are turned on and off as shown in Fig. 4. More specifically, the discontinuous current flow of the SIMO converter generates switching noise (V_{SWN}) from the parasitic inductance in output [11], [18]–[20]. It affects the operation of the comparator directly and causes chaotic operation when there is a very light-load output because the output ripple voltage becomes smaller compared to that of the switching noise [16], [18]. In other words, the ACBC becomes sensitive to the switching noise at light-load output.

In summary, an ACBC offers many advantages, such as fast transient response and low cross regulation, for the outputs under heavy-load conditions. However, an ACBC is not suitable when light-load outputs exist due to regulation problems, switching noise, and efficiency degradation.

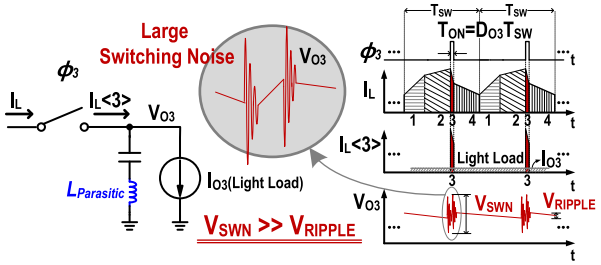

FIGURE 4. Switching noise issue with parasitic inductance in output.

B. ADAPTIVE PULSE MODULATION CONTROL

To resolve the problems occurring with light-load outputs in an ACBC, a pulse skip mode can be inserted [18]. However, when the number of the light-load output increased, it can cause stability issues due to chaotic sequence powering. As an alternative method, APM control, which supplies energy to the most urgent output with the largest error using a maximum error selector, as shown in Fig. 5, was presented in [16]. In this control method, the output switching frequency varies depending on the load condition, but this approach is also associated with some problems with heavy-load outputs.

1) *Irregular Switching*
In APM control, the output switching frequency variation, which is dependent on the load current, also causes irregular switching. Such irregular switching makes the frequency spectrum distributed, and the resultant EMI for heavy-load powering becomes hard to filter out, potentially causing serious problems for mobile applications as shown in Fig. 6 (a) and potentially even failing to meet the EMI specifications [22].

2) *Large Output Voltage Ripple*
When utilizing an APM control method, non-periodic output switching of heavyload outputs causes cross regulation to occur even in steady state. Due to such cross regulation, large ripple voltage is observed not only in a single switching cycle but also throughout multiple cycles as shown in Fig. 6 (b).

In summary, APM control offers advantages such as efficiency improvement and good regulation performance under light-load conditions. However, it is not suitable under heavy-load conditions due to irregular switching and large ripple voltage.

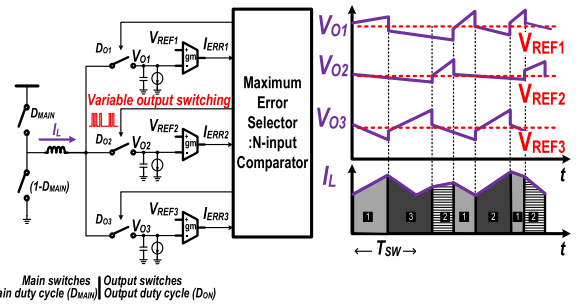

FIGURE 5. SIMO converter with APM control.

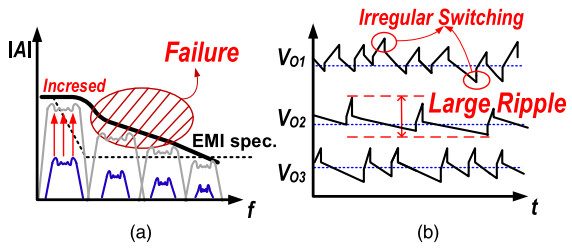

FIGURE 6. (a) EMI problem and (b) large ripple problem in SIMO converter with APM control.

C. DIVERSIFIED LOAD CONDITION

Due to unpredictable variation of the load current, the SIMO converter generally operates under unbalanced load condition as shown in Fig. 7. An unbalanced load condition that has large differences in the load currents is defined as a diversified load condition. In practical use, this diversified load condition occurs frequently. Therefore, SIMO converters must operate well in such condition. However, except for the severe regulation problems described above, when utilizing only one SIMO converter with varying load conditions, the efficiency can be sharply degraded. To analyze the power efficiency of a SIMO converter with an ACBC, the total output power (P_{OUT}) is expressed as follows:

$$P_{OUT} = \sum_{1}^{N} I_{Oi} V_{Oi} = (I_{O1} V_{O1} + I_{O2} V_{O2} + \cdots + I_{ON} V_{ON}) \tag{4}$$

where I_{Oi} and V_{Oi} are the load current and the output voltage, respectively, for each output. When using a buck-type SIMO converter, I_L is the sum of all of the load currents.

$$I_L = I_{O1} + I_{O2} + \cdots + I_{ON} \tag{5}$$

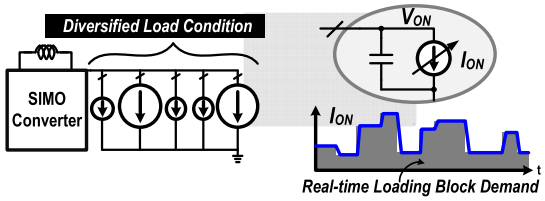

FIGURE 7. SIMO converter in diversified load condition.

Meanwhile, we assume that current ripple of I_L is negligible for the simple calculation. Thus, the conduction loss (P_{COND}) in a SIMO converter can be written as follows:

$$P_{COND} = D_{MAIN} I_L^2 R_{on,p} + (1 - D_{MAIN}) I_L^2 R_{on,n} + \cdots + \sum_{1}^{N} D_{Oi} I_L^2 R_{on,out} \tag{6}$$

where D_{MAIN}, R_{onp}, R_{onn}, and $R_{on,out}$ are the main duty for input switch control, on-resistance of the input PMOS switch, on-resistance of the input NMOS switch, and on-resistance of the output switches. If R_{onn} and R_{onp} are the same value as R_{on}, P_{COND} is rewritten as follows:

$$\begin{aligned} P_{COND} &= (1 + \lambda \sum_{1}^{N} D_{Oi}) I_L^2 R_{on} \\ &= R_{on}(1 + \lambda)(\sum_{1}^{N} I_{Oi})^2 \\ &= R_{on}(1 + \lambda)(I_{O1} + I_{O2} + \cdots + I_{ON})^2 \end{aligned} \tag{7}$$

where λ is the coefficient that shows the relationship between R_{on} and $R_{on,out}$. Eq. (7) shows that P_{COND} is proportional to the square of I_{ON}. Other main power losses, switching loss (P_{SW}) and controller loss (P_{CTRL}), are independent of I_{ON}. The total main power loss (P_{LOSS}) is expressed the sum of each losses as below.

$$P_{LOSS} = P_{COND} + P_{SW} + P_{CTRL}. \tag{8}$$

Also, the efficiency (η_{conv}) of a SIMO converter is expressed as follows:

$$\eta_{conv} = \frac{P_{OUT}}{P_{OUT} + P_{LOSS}} \times 100. \tag{9}$$

Based on (9), Fig. 8 shows the conceptual graphs of the efficiency and power loss in a SIMO converter. The SIMO converter is very sensitive to the load current change of a single output. This will be worse for a SIMO converter under diversified load condition. SIMO converters usually operate outside their peak efficiency region due to unpredictable variation of the load currents. To avoid efficiency degradation and regulation issues under diversified load conditions, heavy-load outputs must be distributed to the ACBC, and light-load outputs must be distributed to the APM control as show in Fig. 9.

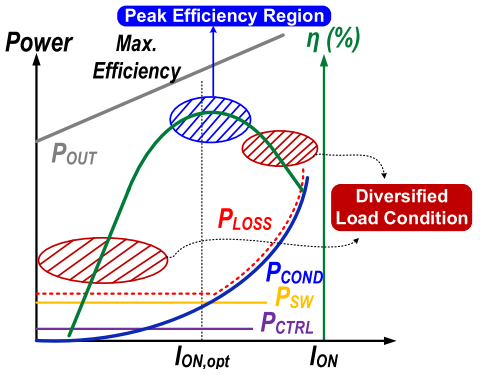

FIGURE 8. Conceptual graphs of the efficiency and power loss in SIMO converter.

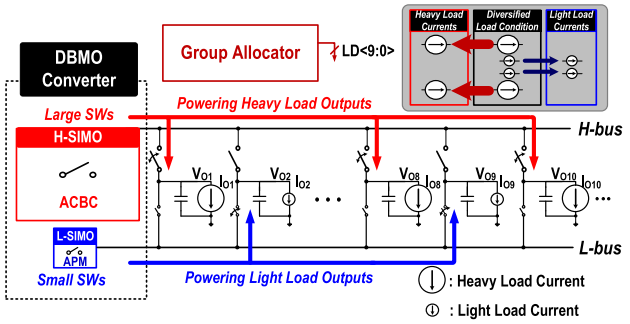

FIGURE 9. Conceptual architecture of DBMO converter.

To balance the load condition, this paper, for the first time, proposes a reconfigurable SIMO system that not only resolves the issues caused by variation in the load current condition of the outputs but also improves the power efficiency.

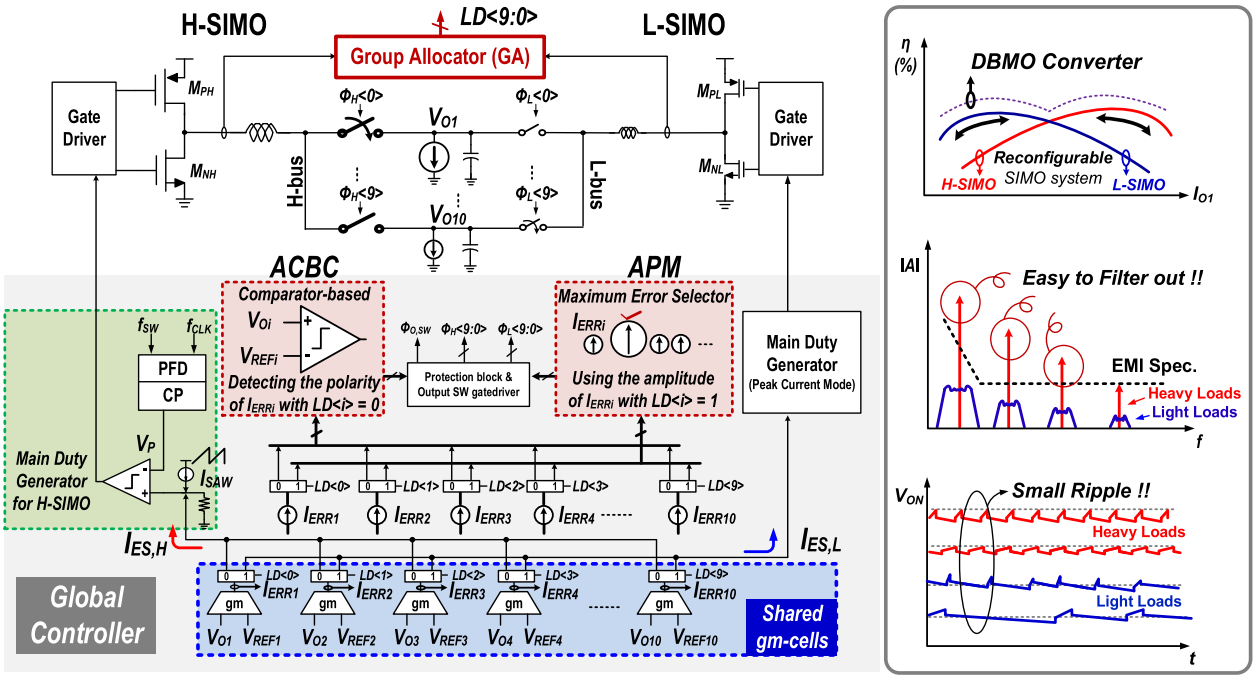

FIGURE 10. Overall structure the advantages of the DBMO converter.

III. PROPOSED DUAL-BUS MULTIPLE-OUTPUT STRUCTURE

A. OVERALL STRUCTURE

Fig. 10 shows the overall structure of the proposed dual-bus multiple-output converter with 10 outputs. There are two buses in the DBMO converter: the H-bus and the L-bus are the power lines coming from heavy-load SIMO converter (H-SIMO) and light-load SIMO converter (L-SIMO), respectively. The group allocator (GA) classifies each load current as heavy or light and properly assigns each output to be connected to either the H-bus or the L-bus such that the load condition of each bus is well balanced. The H-SIMO converter is controlled with an ACBC, appropriate for heavy-load outputs, and the L-SIMO converter is controlled with an APM, appropriate for light-load outputs.

Problems that occur when light-load and heavy-load outputs co-exist are solved by the use of a DBMO converter since the outputs are well distributed to the proper bus according to the load condition. For the H-SIMO converter adopting an ACBC with only heavy load outputs, switching is periodic, and the EMI problem is eased because a single tone generated by the fixed frequency of the output switching operation is easy to filter out. In addition, the minimum on-time problem is resolved since the light-load outputs are not allocated to the H-SIMO converter. Moreover, the ripple voltage of the heavy-load outputs in the H-SIMO converter is large compared to the switching noise caused by parasitic inductance, making the effect of the switching noise insignificant. Lastly, since there is no unnecessary output switching in the H-SIMO converter, unwanted switching loss is reduced.

Meanwhile, since the L-SIMO converter adopts an APM control method with only light-load outputs, although the output switching frequency is adaptive, the frequency spectrum is distributed, and EMI specifications are met because the power level is low [22]–[24]. In addition, steady state cross regulation is minimized, and the large ripple voltage observed throughout multiple cycles disappears since there is no heavy-load output in the L-SIMO converter. Consequently, the DBMO converter in the proposed SIMO system can resolve most of the aforementioned practical issues associated with SIMO converters.

B. LIGHTLOAD SIMO CONVERTER

The GA judges whether a load is heavy or light and generates a 10-bit table (‘LD< 9 : 0 >’); ‘0’ means heavyload current and ‘1’ means lightload current. The lightload outputs judged by the GA are connected to the L-bus to be included in the L-SIMO converter. Among the ten gm-cells shared by the H-SIMO and L-SIMO converters, the gm-cells allocated to the lightload output (LD< n >= 1) generate the lightload output error currents and the currents are summed to produce the total lightload error current ($I_{ES,L}$). The main duty of the L-SIMO converter is controlled so that $I_{ES,L}$ becomes zero in peak-current mode control. Since the L-SIMO utilizes APM control, the error of each output is continuously monitored, and I_L is supplied to the most urgent output, resulting in variable output switching frequency.

C. HEAVYLOAD SIMO CONVERTER

The heavy-load outputs, as judged by the GA, are connected to the H-bus to be included in the H-SIMO converter.

Among the ten shared gm-cells, the gm-cells allocated to the heavy-load output (LD<n>=0) generate the heavy-load output error currents, and the currents are summed to produce the total heavy-load error current ($I_{ES,H}$). The main duty of the H-SIMO converter is controlled so that $I_{ES,H}$ becomes zero. The regulation is self-controlled by monitoring the sign of the gm-cells allocated to the H-bus, like a comparator.

D. RECONFIGURABLE STRUCTURE

Since the GA continuously senses and judges the output load current and distributes the outputs to the appropriate converter, either to the H-SIMO with large-size switches or the L-SIMO with small-size switches, the structure of the converter varies, i.e., the converter is reconfigured depending on the load condition of the outputs. Therefore, severe power efficiency degradation can be prevented in diversified load conditions, and the converter can achieve high efficiency across a wide range of load currents.

IV. CIRCUIT IMPLEMENTATION

A. INDIRECT LOAD CURRENT SENSING TECHNIQUE

To distribute the outputs properly, the load current sensor is an essential block. To sense the load currents of N outputs, N load current sensors are required as shown in Fig. 11 (a), causing large power consumption and increased complexity and size of the system [25]. The indirect load current sensing method utilizing a time-interleaved scheme solves this problem by enabling only one GA as a load sensor as shown in Fig. 11 (b).

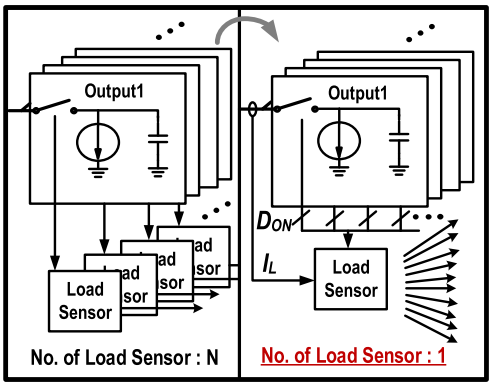

FIGURE 11. (a) Conventional load sensor and (b) the proposed load sensor for multiple outputs.

For indirect sensing of the load current I_{ON}, both the inductor current information and the output on-duty D_{ON} information are required.

$$D_{ON} I_L(t) = I_{ON} \tag{8}$$

Fig. 12 (a) shows the indirect inductor current-sensing method. When an RC filter with a series-connected resistor (R_F) and a capacitor (C_F) is connected in parallel with an inductor (L), the relationship between the voltage across C_F (V_C) and the voltage across L (V_L) is expressed as below:

$$V_C(s) = \frac{V_L(s)}{1 + sR_F C_F} = \left(\frac{1 + sL/R_F}{1 + sR_F C_F}\right) R_{DCR} I_L(s)$$
$$= \left(\frac{1 + sT}{1 + sT_1}\right) R_{DCR} I_L(s) \tag{9}$$

where R_{DCR}, T, T_1, are the parasitic resistance of L, time constant of L and R_{DCR}, and time constant of R_F and C_F, respectively. From (9), if the two time constants are the same ($T = T_1$), the emulated inductor current can be extracted from V_C, which is also the input of the inductor current-sensing OTA. The emulated current flows at the outputs of OTA.

To extract the information about the output duty cycle, another indirect method is used as shown in Fig. 12 (b). Small switches are placed at the outputs of OTA so that they are synchronized with the SIMO converter output power switches. For example, when the H-SIMO converter operates, the small switch sw'_{H1} in the controller is on and off in synchronization with the power switch $SW_{H1}$for V_{O1} when the target output is V_{O1}. As a result, the pieced current (I_{PIECE}) with I_{O1} information can be obtained. This switching operation is repeated continuously for multiple cycles. Here, the inductor current sensing OTA is implemented in a folded cascade structure as shown in Fig. 13. To eliminate its input offset, a chopper technique is applied for accurate current sensing. Simulation result shows that the OTA offset (V_{OS}) is cancelled. During a dead-time interval to avoid the outputs being shorted to each other, the input nodes of OTA can be charged high voltage over VDD like voltage spike. Due to this voltage spike, to prevent a body diode of the chopping switches from turning on, the switches are implemented as NMOS with body switching.

Fig. 12 (c) shows how to determine if a load current is heavy or light load. The I_{PIECE} is supplied to C_{FILT} repetitively for multiple cycles with only sw'_{H1} active while the other switches in the controller are all in the off state. When sw'_{H1} is in the off state, the output of OTA is connected to a reference voltage V_{GA} to enable fast voltage recovery for the next switching. The charged C_{FILT} by I_{PIECE} is discharged by OTA $_F$, which is a buffer-configured OTA that generates a buffered current that indirectly indicates the target I_{O1}. Here, this buffered current is smoothed with low ripple because of C_{FILT} and the limited bandwidth of the buffer. This buffered current is then amplified tenfold using a current mirror. The resultant current (I_{SEN}) is compared to a pre-defined threshold current I_{BD} using a hysteresis current comparator and judged to update the heavy and light load results table (LD<0>). This hysteresis comparator is used to compare I_{SEN} with I_{BD} to eliminate unstable operation when the two currents are of a similar level. After the judgment of LD<0>, GA repeats the above operation for the other target output one by one as shown in the timing diagram in Fig. 14. Simulation results show that this indirect current sensing method works well depending on the load current level in both ACBC with a fixed frequency and APM control with variable frequency in Fig. 15.

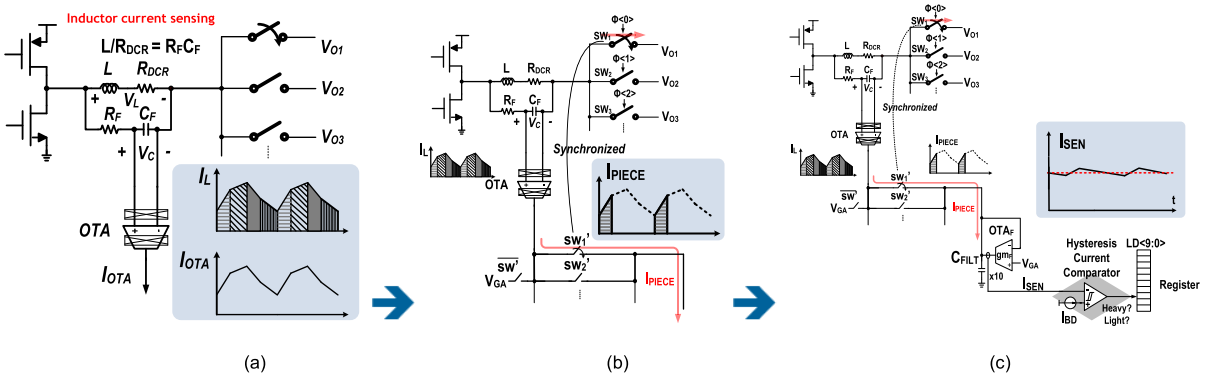

FIGURE 12. (a) Indirect current sensing method with RC filter, (b) Output duty sensing method with synchronized small switch, (c) decision process when the target output is V_{O1}.

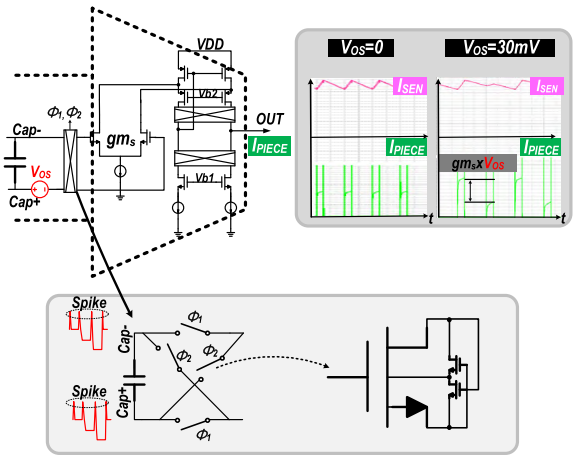

FIGURE 13. Inductor current sensing OTA with a chopping technique.

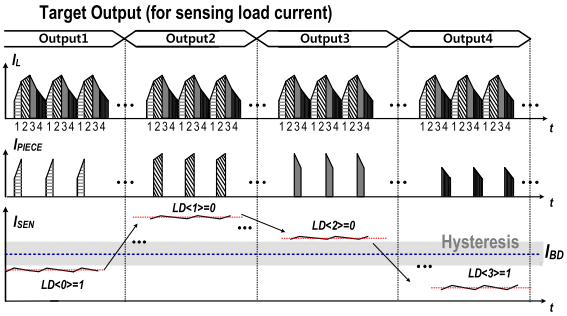

FIGURE 14. Timing diagram of sensing target load current in group allocator.

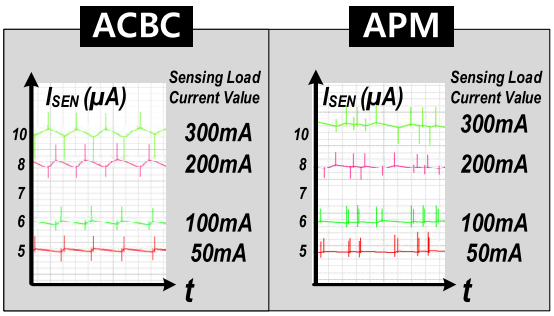

FIGURE 15. Simulation result of indirect sensing method in ACBC and APM control.

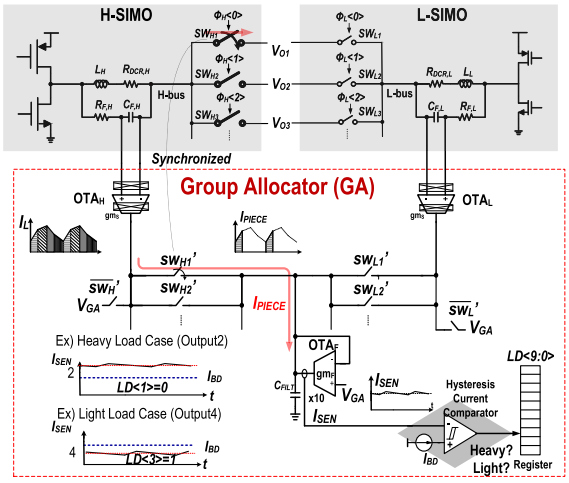

FIGURE 16. Overall structure of the group allocator.

Fig. 16 shows the overall structure of the GA with the two SIMO converters. Since there is only one load current sensor for multiple outputs, the proposed method is simple and power efficient.

The transfer function (A_G(s)) from V_C to I_{SEN} and the design parameters for GA are expressed below.

$$I_{SEN}(s) = K\, g_{mS}\,(\frac{1}{sC_{FILT}} \parallel \frac{1}{g_{mF}})V_C(s), \tag{10}$$

$$A_G(s) = \frac{I_{SEN}(s)}{V_C(s)} = \frac{Kg_{mS}}{g_{mF}} \cdot \frac{1}{1 + sC_{FILT}/g_{mF}}, \tag{11}$$

$$= A_G \frac{1}{1 + s/w_P} \tag{12}$$

where

$$w_P = g_{mF}/C_{FILT} \tag{13}$$

$$A_{G,DC} = Kg_{mS}/g_{mF} \tag{14}$$

$$w_{GB} = A_{G,DC} w_P = Kg_{mS}/C_{FILT} < w_{SW}. \tag{15}$$

Also, g_{mS}, g_{mF}, K, $A_{G,DC}$, w_{GB}, w_P, and w_{sw} are the transconductance of the inductor current sensing OTA (OTA_L and OTA_H), transconductance of OTA_F, current mirror gain, DC value of $A_G(s)$, unit gain bandwidth of $A_G(s)$, 3dB bandwidth of $A_G(s)$, and switching frequency, respectively. Here, w_{GB} should be much smaller than w_{SW} as shown in (15) because the ripple current of I_{SEN} should be reduced to acquire DC-like current for accurate current judgment. Accordingly, because of the limitation of w_{GB}, g_{mS} should be designed to be small to reduce C_{FILT}. As g_{mS} is reduced, g_{mF} should also be designed to be small for acquiring large I_{SEN} through A_G. Therefore, in the design of the GA, the OTAs for each SIMO converter were designed to have small g_{mS} to reduce C_{FILT} and obtain stable I_{SEN}.

B. MAIN DUTY GENERATOR OF H-SIMO CONVERTER

The main duty generator of the L-SIMO converter is implemented with conventional peak current mode control [16]. In contrast, the main duty generator of the H-SIMO converter presented in this paper has a simple design. Fig. 17 (a) shows the block diagram of the H-SIMO controller. The $I_{ES,H}$, which is the error sum of the heavy-load outputs in Fig. 10, is combined with the sawtooth current (I_{SAW}) generated from the sawtooth voltage (V_{SAW}), and the combined current is compared to V_P after converting it to voltage. Therefore, in the steady state, a constant duty is generated because $I_{ES,H}$ is almost zero in this state, where V_P is controlled so that the output switching frequency f_{SW} is locked to a fixed reference frequency f_{REF} by PFD and CP.

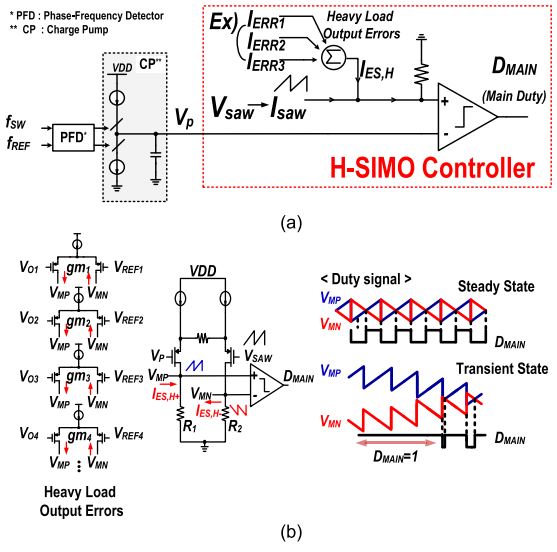

FIGURE 17. (a) Simplified block diagram and (b) the circuit implementation of H-SIMO main switch controller.

Fig. 17 (b) shows the circuit implementation. It has two branches of the main differential pair with two inputs, V_{SAW} and V_P, connected to two differential output resistors (R_1, R_2) and also connected to two branches of the differential pair in each gm-cell allocated to the heavy-load outputs.

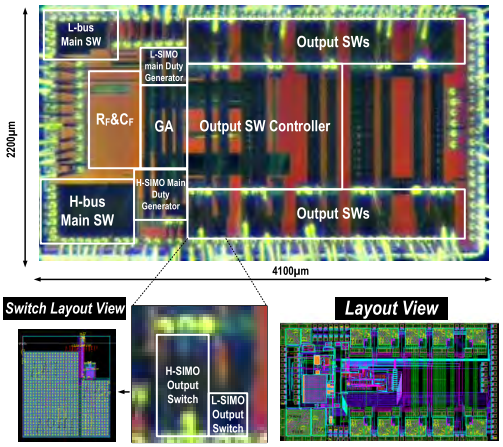

FIGURE 18. Chip micrograph and laout view of DBMO converter.

Therefore, the differential error currents of heavy-load outputs are summed to be $I_{ES,H+}$ and $I_{ES,H-}$ at V_{MP} and V_{MN} nodes, respectively. Dual sawtooth voltages (V_{MP} and V_{NP}) are generated when the two currents ($I_{ES,H+}$, $I_{ES,H-}$) flow through R_1 and R_2, and the main duty signal is generated by comparing these dual sawtooth voltages. Therefore, an ACBC with fixed frequency can be simply implemented. Furthermore, a fast response in the transient state can be achieved since the highly increased $I_{ES,H}$ in the transient state always makes the comparator output high (D_{MAIN} =1) until $I_{ES,H}$ has a sufficiently low level of error.

C. DESIGN CONSIDERATION FOR SIZING SWITCHES AND BOUNDARY CURRENT

In this paper, we implemented a DBMO converter that includes two SIMO converters. There are many ways to design this SIMO system. For example, in our design, we first set the optimal load current at the outputs of each SIMO converter. The optimal load current of the H-SIMO converter ($I_{ON,OPTH}$) is set N times larger than that of the L-SIMO converter ($I_{ON,OPTL}$) as described below:

$$I_{ON,OPTH} = NI_{ON,OPTL}. \tag{16}$$

The switching loss for gate driving in the L-SIMO converter ($P_{SW,L}$) is expressed as follows:

$$P_{SW,L} = C_{gate}V_{DD}^2 f_{SW,opt} = \alpha WLC_{OX}V_{DD}^2 f_{SW,opt} \tag{17}$$

where V_{DD}, C_{gate}, C_{OX}, α, W, L and $f_{SW,opt}$ are the battery voltage, gate capacitance, oxide capacitance, coefficient of gate capacitance, power switch width, power switch length, and switching frequency in optimal design, respectively. Note that $P_{SW,L}$ is proportional to W. Meanwhile, the conduction loss ($P_{COND,L}$) in the L-SIMO converter is expressed as follows:

$$P_{COND,L} = D_{ON}I_{L,RMS}^2 R_{on} = \frac{D_{ON}I_{L,RMS}^2}{\mu C_{OX}\frac{W}{L}(V_{GS} - V_{TH})} \tag{18}$$

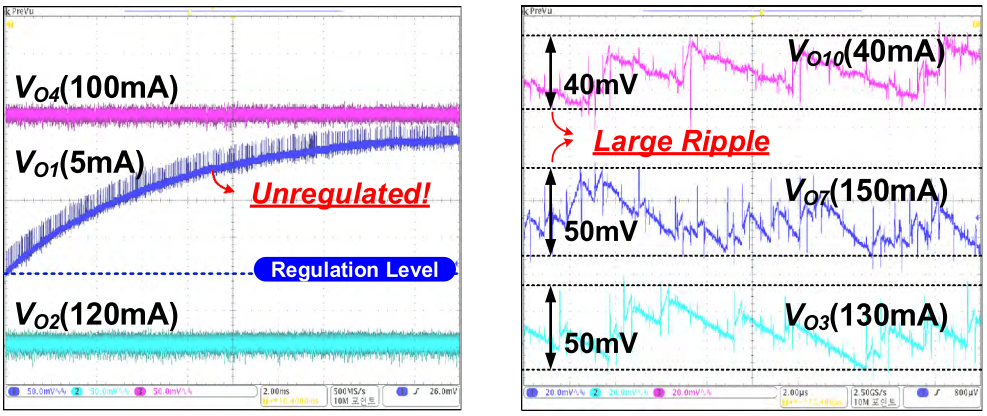

(a) (b)

FIGURE 19. Regulation problems in (a) ACBC and (b) APM control with diversified load condition.

where $I_{L,RMS}$, μ, V_{GS}, and V_{TH} are the root mean square value of I_L, mobility, gate to source voltage, and threshold voltage of the power switches, respectively. Note that $P_{COND,L}$ is inversely proportional to W. Although there are other losses, $P_{SW,L}$ and $P_{COND,L}$ are the dominant losses. These losses are set at the same value for maximum efficiency.

$$P_{COND,L}(W_{opt,L}) = P_{SWloss,L}(W_{opt,L}). \tag{19}$$

From (19), we can obtain the optimal width of the power switch ($W_{opt,L}$) with minimum L. Using this $W_{opt,L}$ as a unit, the H-SIMO converter can be designed in the same manner. Then, the relationship between conduction loss ($P_{COND,H}$) and switching loss ($P_{SW,H}$) in the H-SIMO converter is expressed as follows:

$$P_{COND,H}(W_{opt,H}) = P_{SW,H}(W_{opt,H}), \tag{20}$$

$$N^2 \frac{W_{opt,L}}{W_{opt,H}} P_{COND,L}(W_{opt,L}) = \frac{W_{opt,H}}{W_{opt,L}} P_{SW,L}(W_{opt,L}) \tag{21}$$

$$W_{opt,H} = NW_{opt,L}. \tag{22}$$

Eq.(22) shows the N times larger power switch in H-SIMO converter than that in L-SIMO converter should be required. Moreover, $I_{BD,L}$, which determines the real boundary current, is set to the mean of both $I_{ON,OPTH}$ and $I_{ON,OPTL}$:

$$I_{BD,L} = \frac{(N+1)}{2} I_{OPT,L} = \beta I_{BD}. \tag{23}$$

where β is the scaling factor of $I_{BD,L}$ to compare scaled I_{BD} with I_{SEN} with small current level for reducing power consumption in the GA.

In our SIMO system design, we set the following parameters: $N = 3$, $I_{OPT,L} = 50$ mA, $I_{OPT,H} = 150$ mA, and $I_{BD,L} = 100$ mA. With this different power switch sizing, each SIMO converter can achieve high efficiency across a wide load range.

V. MEASUREMENT RESULTS

The proposed 10-output DBMO converter is fabricated with a 1P4M 0.18 um CMOS process. The chip micrograph and layout view with die area of 2.2 mm × 4.1 mm are shown in Fig. 18. The output switches of the H-SIMO converter were designed three times larger than those of the L-SIMO converter in this work as mentioned in the design considerations. The outputs V_{O1} through V_{O10} are regulated to 1.8 V, 1.8 V, 2.5 V, 2.8 V, 3.3 V, 1.8 V, 2.5 V, 2.8 V, 2.8 V and 3.3 V, respectively.

The waveforms in Fig. 19 demonstrate the motivation for this work by showing the regulation problems of a conventional SIMO converter under diversified load condition. With very light-load output, the ACBC results in regulation failure due to a minimum on-time problem (Fig. 19 (a)). With diversified load conditions and APM control, large ripple results due to steady state cross regulation caused by irregular switching as shown in Fig. 19 (b).

Fig. 20 shows the regulation performance achieved with the well-balanced load condition produced by the GA in steady state. Owing to the load balancing function, the H-SIMO converter with an ACBC exhibits no regulation problem and operates well with a fixed frequency as shown in Fig. 20 (a). The L-SIMO converter with APM control has small ripple with minimized steady state cross regulation and shows adaptive output switching frequency depending on the load current as shown in Fig. 20 (b). All the ripples have small values below 25 mV in the outputs of the DBMO converter.

Fig. 21 shows the bus change operation of the target output V_{O6} using the GA. To show the output bus change from H-bus to L-bus, V_{O6} was initially connected to H-bus, and I_{O6} was set to 90 mA, which is smaller than $I_{BD,L}$ (100 mA). Fig. 21 (a) shows that the target output V_{O6} is clearly changed from H-bus to L-bus. In contrast, to show the output bus change from L-bus to H-bus, V_{O6} was initially connected to L-bus, and I_{O6} was set to 120 mA, which is larger than $I_{BD,L}$. Fig. 21 (b) shows that the target output V_{O6} is clearly changed from L-bus to H-bus. It shows that the output voltages are well regulated after the bus change. The undershoot and overshoot of the output waveforms in the figures are caused by cross regulation due to status change of each bus, resulting

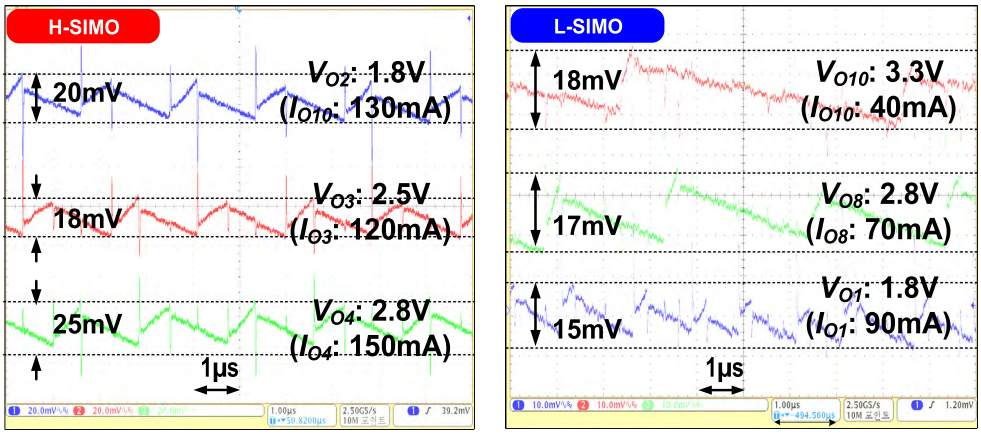

(a) (b)

FIGURE 20. Regulation performance in (a) ACBC and (b) APM control with well-balanced load condition.

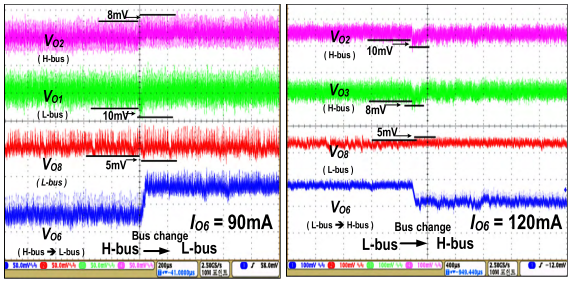

(a) (b)

FIGURE 21. Bus change of V_{O1} (a) from H-bus to L-bus and (b) from L-bus to H-bus.

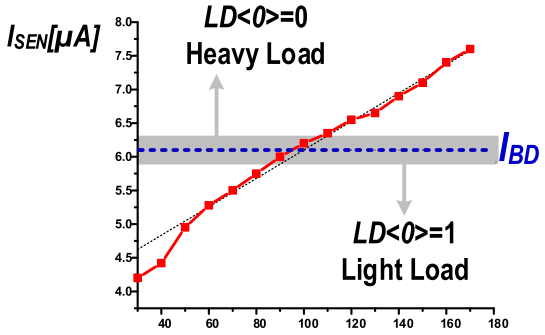

FIGURE 22. Plot of the sensed current by the GA (I_{SEN}) versus its target load current (I_{O1}).

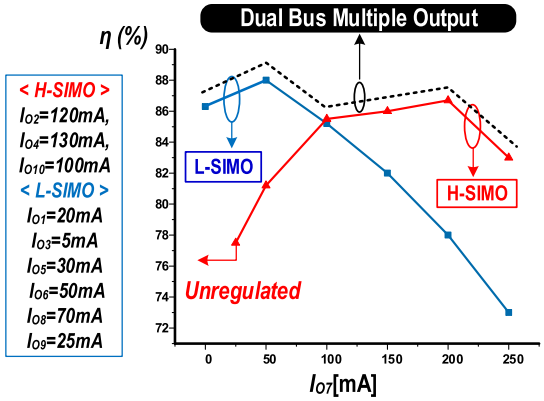

FIGURE 23. Measured efficiency plot of DBMO converter versus load current (I_{O7}).

in 0.2 (mV/mA) for H-bus and 0.17 (mV/mA) for L-bus. There is a difference in the voltage level of V_{O6} after the bus change, which is caused by the load regulation of each SIMO converter and the offsets of gm-cells and comparators [11].

Fig. 22 depicts the current I_{SEN} sensed by the GA from the load current I_{O1} showing good sensing performance. As the value of $LD<0>$ is defined by I_{BD}, the bus of the target output is changed, and the output is distributed to the appropriate controlled SIMO converter. The hysteresis region shown in the figure is inserted to guarantee stable operation even when I_{SEN} is similar to I_{BD}.

Fig. 23 shows the measured efficiency of both SIMO converters versus load current (I_{O7}). The peak efficiencies of

TABLE 1. Performance comparison.

		[11]	[14]	[13]	Proposed	
					H-SIMO	L-SIMO
Process		65nm	0.35μm	0.35μm	0.18μm	
Topology		6 Buck outputs	4 Buck outputs	5 Buck outputs	10 DBMO outputs	
Supply Voltage(V)		5.0	2.7 - 5.0	3.4 - 4.3	5.0	
Frequency		2MHz	1MHz	1.2MHz	1MHz	
Voltage Ripple		< 25mV	< 30mV	< 40mV	< 25mV	
Inductor & Capacitor		4.7μH & 10μF	4.7μH & 10μF	2.2μH & 10μF	4.7μH & 10μF	
Control Method	Heavy Load	PMB Control	ACBC	Charge Control	ACBC	
	Light Load	-	-	Pulse skip	APM	
Load Transient (mV/mA)		0.93	0.16	0.6	0.19	0.17
Cross Regulation (mV/mA)		0.31	0.04	0.067	0.088	0.1
Max. Efficiency		-	87%	83.1%	86.7%	88%
Load Balancing Function		Unsupportable	Unsupportable	Unsupportable	Supportable 0-100mA : L-bus 100mA-300mA: H-bus	
Allowable Load Range		-	-	-	0mA - 300mA	
Load Independency in Efficiency		Low	Low	Low	High	
Max. Output Power(W)		2.16	1.2	2.232	2.83	

the H-SIMO and L-SIMO converters are 86.7% and 88%, respectively. For the L-SIMO converter, the power efficiency is dramatically degraded when I_{O7} becomes a heavy-load. For the H-SIMO converter, the efficiency degrades abruptly when I_{O7} becomes a light-load, and the converter could malfunction with very light-load I_{O7}. In other words, conventional SIMO converters have low efficiency under diversified load

condition. In contrast, thanks to the load balancing function, the proposed DBMO converter as a new SIMO system achieves over 81% efficiency over a wide load range (0 mA–300 mA). Table I compares the performance of the proposed DBMO converter with previous works. Since it supports the load balancing function, it extends the allowable load range while maintaining comparable peak efficiency, load transient response and small ripple with 10-output.

VI. CONCLUSION

This paper presents a 10-output DBMO converter with load balancing function as a new SIMO powering system. The outputs with different load conditions are properly distributed by the proposed indirect load current sensing method utilizing a time-interleaved scheme. It enables efficient and simple load current sensing of multiple outputs through only one GA. The heavy-load outputs are assigned to the H-SIMO converter with an ACBC and large sized switches. The light-load outputs are assigned to the L-SIMO converter with APM control and small-sized switches. Such proper allocation of the outputs depending on their load condition resolves the practical regulation issues associated with a conventional SIMO converter and improves the power efficiency. Moreover, the DBMO converter achieves an allowable load range of 0 mA–300 mA with greater than 81% efficiency throughout the whole load range due to the reconfigurable SIMO system with dual buses.

REFERENCES

[1] K. E. L. Marcillo *et al.*, "Interval robust controller to minimize oscillations effects caused by constant power load in a DC multi-converter buck-buck system," *IEEE Access*, vol. 7, pp. 26324–26342, 2019.
[2] X. Jin, L. Wang, D. Yu, Y. Geng, and R. Xu, "Pulse train controlled single input dual-output buck converter with coupled inductors," *IEEE Access*, vol. 6, pp. 41504–41517, 2018.
[3] J.-M. Chang and M. Pedram, "Energy minimization using multiple supply voltages," *IEEE Trans. Very Large Scale Integr. (VLSI) Syst.*, vol. 5, no. 4, pp. 436–443, Dec. 1997.
[4] C. F. Bassetti, "Method and apparatus for image based power control of drive circuitry of a display pixel," U.S. Patent 0 008 297 A1, Jan. 11, 2007.
[5] B. H. Calhoun and A. P. Chandrakasan, "Ultra-dynamic voltage scaling (UDVS) using sub-threshold operation and local voltage dithering," *IEEE J. Solid-State Circuits*, vol. 41, no. 1, pp. 238–245, Jan. 2006.
[6] M.-Y. Jung, S.-U. Shin, and G.-H. Cho, "Issues of single-inductor multiple-output DC-DC converters," in *Proc. SoC Design Conf.*, Nov. 2015, pp. 115–116.
[7] D. Ma, W.-H. Ki, and C.-Y. Tsui, "A pseudo-CCM/DCM SIMO switching converter with freewheel switching," *IEEE J. Solid-State Circuits*, vol. 38, no. 6, pp. 1007–1014, Jun. 2003.
[8] J. Jia and K. N. Leung, "Digital-control single-inductor triple-output DC–DC converter with pre-sub-period inductor-current control," *IEEE Trans. Power Electron.*, vol. 27, no. 4, pp. 2028–2042, Apr. 2012.
[9] X. Jing, P. K. T. Mok, and M. C. Lee, "A wide-load-range constant-charge-auto-hopping control single-inductor-dual-output boost regulator with minimized cross-regulation," *IEEE J. Solid-State Circuits*, vol. 46, no. 10, pp. 2350–2362, Oct. 2011.
[10] H.-P. Le, C.-S. Chae, K.-C. Lee, S.-W. Wang, G.-H. Cho, and G.-H. Cho, "A single-inductor switching DC–DC converter with five outputs and ordered power-distributive control," *IEEE J. Solid-State Circuits*, vol. 42, no. 12, pp. 2706–2714, Dec. 2007.
[11] K.-C. Lee, C.-S. Chae, G.-H. Cho, and G.-H. Cho, "A PLL-based high stability single-inductor 6-channel output DC-DC buck converter," in *IEEE Int. Solid-State Circuits Conf. (ISSCC) Dig. Tech. Papers*, Feb. 2010, pp. 200–201.
[12] K.-S. Seol, Y.-J. Woo, G.-H. Cho, G.-H. Cho, J.-W. Lee, and S.-I. Kim, "Multiple-output step-up/down switching DC-DC converter with vestigial current control," in *IEEE Int. Solid-State Circuits Conf. (ISSCC) Dig. Tech. Papers*, Feb. 2009, pp. 442–443.
[13] C.-W. Kuan and H.-C. Lin, "Near-independently regulated 5-output single-inductor DC-DC buck converter delivering 1.2 W/mm^2 in 65 nm CMOS," in *Proc. IEEE Int. Solid-State Circuits Conf.*, Feb. 2012, pp. 274–276.
[14] D. Lu, Y. Qian, and Z. Hong, "4.3 An 87%-peak-efficiency DVS-capable single-inductor 4-output DC-DC buck converter with ripple-based adaptive off-time control," in *Proc. IEEE Int. Solid-State Circuits Conf. (ISSCC) Dig. Tech. Papers*, Feb. 2014, pp. 82–83.
[15] T. Y. Goh and W. T. Ng, "Single discharge control for single-inductor multiple-output DC–DC buck converters," *IEEE Trans. Power Electron.*, vol. 33, no. 3, pp. 2307–2316, Mar. 2018.
[16] M.-Y. Jung, S.-H. Park, J.-S. Bang, D.-C. Park, S.-U. Shin, and G.-H. Cho, "An error-based controlled single-inductor 10-output DC-DC buck converter with high efficiency at light load using adaptive pulse modulation," in *IEEE Int. Solid-State Circuits Conf. (ISSCC) Dig. Tech. Papers*, Feb. 2015, pp. 1–3.
[17] Y. Jang and M. M. Jovanovic, "Light-load efficiency optimization method," *IEEE Trans. Power Electron.*, vol. 25, no. 1, pp. 67–74, Jan. 2010.
[18] D. Park, T.-H. Kong, S. Choi, and G.-H. Cho, "An 83% peak efficiency and 1.07 W/mm^2 power density single inductor 4-output DC-DC converter with bang-bang zeroth-order control," in *Proc. IEEE Asian Solid-State Circuits Conf.*, Nov. 2014, pp. 61–64.
[19] B. Bae, Y. Shim, K. Koo, J. Cho, J. S. Pak, and J. Kim, "Modeling and measurement of power supply noise effects on an analog-to-digital converter based on a chip-PCB hierarchical power distribution network analysis," *IEEE Trans. Electromagn. Compat.*, vol. 55, no. 6, pp. 1260–1270, Dec. 2013.
[20] K. Koo *et al.*, "Modeling and analysis of power supply noise imbalance on ultra high frequency differential low noise amplifiers in a system-in-package," *IEEE Trans. Adv. Packag.*, vol. 33, no. 3, pp. 602–616, Aug. 2010.
[21] S.-U. Shin *et al.*, "A reconfigurable SIMO system with 10-output dual-bus DC-DC converter using the load balancing function in group allocator for diversified load condition," in *Proc. IEEE Symp. VLSI Circuits*, Jun. 2016, pp. 1–2.
[22] L.-J. Chen and K.-H. Lin, "Implementation of a compact EMI filter array for 4G-LTE applications on LTCC," *IEEE Trans. Compon., Packag., Manuf. Technol.*, vol. 5, no. 6, pp. 713–722, Jun. 2015.
[23] F. Mihali and D. Kos, "Reduced conductive EMI in switched-mode DC–DC power converters without EMI filters: PWM versus randomized PWM," *IEEE Trans. Power Electron.*, vol. 21, no. 6, pp. 1783–1794, Nov. 2006.
[24] O. Trescases, G. Wei, A. Prodic, and W. T. Ng, "An EMI reduction technique for digitally controlled SMPS," *IEEE Trans. Power Electron.*, vol. 22, no. 4, pp. 1560–1565, Jul. 2007.
[25] A. V. Peterchev and S. R. Sanders, "Load-line regulation with estimated load-current feedforward: Application to microprocessor voltage regulators," *IEEE Trans. Power Electron.*, vol. 21, no. 6, pp. 1704–1717, Nov. 2006.

SE-UN SHIN received the B.S. degree in electronics engineering from Kyungpook National University, Daegu, South Korea, in 2013, and the M.S. and Ph.D. degrees in electrical engineering from the Korea Advanced Institute of Science and Technology (KAIST), Daejeon, South Korea, in 2019.

He is currently a Postdoctoral Scholar with the University of Michigan. His current research interests include analog integrated circuit design and power management IC design, including energy harvesting, battery charger, wireless power transfer systems, switched capacitor/inductive converters, and hybrid converter topology. He was a recipient of the 2017 and 2018 IEEE Solid-State Circuits Society Predoctoral Achievement Award.